Accurate pseudopotential local-density-approximation computations for neutral and ionized dimers of the IB and IIB groups

Pietro Ballone*
Institut Romand de Recherche Numérique en Physique des Matériaux (IRRMA), PHB-Ecublens, 1015 Lausanne, Switzerland

Giulia Galli†
Department of Physics and Material Research Laboratory, University of Illinois at Urbana Champaign, Urbana, Illinois 61801

(Received 12 February 1990)

We have implemented an efficient algorithm to compute properties of linear molecules in the pseudopotential local-density-approximation (LDA) framework. Orbitals are expanded in an orthogonal and complete basis set of cylindrical waves. A large number of basis functions is dealt with using an iterative procedure requiring a number of operations proportional to the size of the basis set to the power $\frac{3}{2}$. This favorable scaling law makes it possible to approach the LDA limit for molecules with s, p, and d valence electrons. We present results for homonuclear dimers of the IB and IIB elements. Comparison with previous computations for the IB dimers points out the advantages of our extended and unbiased basis set. We show that the LDA is able to account for many of the qualitative features characterizing the bonding of the IIB dimers, although important quantitative discrepancies remain in the comparison with experiment. Finally, we investigate the role of the closed-shell d electrons in the bonding of all these molecules.

I. INTRODUCTION

Density-functional theory[1] (DFT) in the local-density approximation[2] (LDA) has made possible the microscopic understanding and predictions of a variety of properties of real materials. As far as extended systems are concerned, a number of recent papers[3,4] review the successes (and occasional failures) of DFT-LDA in predicting equilibrium geometries, vibrational spectra, and phase diagrams under pressure of both metal and semiconductors. Finite systems, such as molecules or clusters, are slightly less explored within the LDA framework. However, a growing number of computations,[4,5] indicate that LDA also offers a satisfactory picture of the chemical bond for these small systems. Furthermore, in predicting ground-state properties LDA is usually superior to the self-consistent-field Hartree-Fock (SCF-HF) scheme, and, by far, computationally less demanding than configuration-interaction (CI) methods.

Recently interest in molecular applications has been focused on systems containing transition-metal atoms, for which theories are severely tested by the combined problems due to many valence electrons, important relativistic effects, and the interplay between localized d and extended s states. For these systems, a precise assessment of the merits and limitations of LDA (and other approximations) is hindered by computational problems that are specific to molecular applications. For instance, the powerful technique of plane-wave expansion, adopted in most total-energy computations for solids, is not convenient for isolated molecules, since very large unit cells are required for the computation of their properties. In order to simplify the numerical task, many of the early LDA calculations for molecules introduced shape (muffin-tin) approximations for the potential. Although reliable for the compact structures of many crystals, these approximations lead to qualitatively wrong results for some molecules.[6] Most of the recent computations rely on a different kind of approximation: The LDA single-particle orbitals are expanded in a small set of localized basis functions. Although these methods are believed to be accurate, the final answer on their quality must come from a computation not suffering from strong limitations on the basis set.

Dimers of the IB and IIB elements are important benchmarks for theories and computational methods aiming to describe transition-metal molecules. These two families of dimers display a remarkable variety of properties, going from the strong cohesion of Cu_2, Ag_2, and Au_2 to the weak van der Waals bonding of Zn_2, Cd_2, and Hg_2. Upon ionization, the Group IIB dimers show a dramatic increase of cohesion, with D_e jumping by roughly a factor of 20. Due to technical problems, few experimental data are available for ionized dimers of the IB elements. However, these systems are also known to have interesting properties, such as the intriguing stability of Au_2^{2+}.[7]

In order to perform accurate LDA computations for some of these systems, we have implemented a new algorithm, tailored for LDA-pseudopotential calculations for linear molecules.[8] This algorithm, derived from the well-known computational scheme of Car and Parrinello,[9] has two main innovative features. The LDA molecular orbitals are expanded in an orthogonal and complete basis set (cylindrical waves) adapted to the symmetry of the Hamiltonian. The large number of basis functions required by this expansion (up to 2^{14} for Cu_2, Zn_2, and the

ionized dimers) is dealt with using an efficient iterative procedure.

Results obtained with our scheme for mercury dimers have been published recently.[8] Here we give a more complete account of the method and present a systematic study for the homonuclear dimers of the Group IB and IIB elements. The main goals of the present computation are (i) to gauge the performances of our extended basis on the IB dimers, for which several LDA studies have already been published; (ii) to perform, for the first time, a systematic LDA computation of the bonding properties of the Group IIB dimers; and (iii) to investigate the role of the closed-shell d electrons in the bonding of these molecules.

Our results confirm the global accuracy of computations based on localized basis functions, especially for the evaluation of equilibrium distances. However, for the IB dimers we compute cohesive energies systematically larger than those reported in previous studies: This points out the importance of an unbiased basis set for molecular computations.

As far as the Group IIB dimers are concerned, we show that LDA is able to reproduce the qualitative features of the bonding of these molecules. However, the quantitative comparison with experiments is not satisfactory. Cohesive energies are overestimated by roughly a factor of 3 and interatomic distances are underestimated by nearly 10%.

In Ref. 8 we have shown that the $5d^{10}$ electrons of mercury play an important role in determining the bonding parameters of Hg_2. Moreover, we have shown that their effect can be approximated, to a reasonable accuracy, by including in the pseudopotential corrections due to the nonlinearity of the exchange-correlation energy.[10] Here we extend our analysis to Zn_2 and Cd_2.

II. METHOD

As mentioned in the Introduction, the DFT-LDA offers a reliable and efficient scheme to compute the ground-state properties of many-electron systems. In the Born-Oppenheimer approximation, the set of ionic coordinates $\{\mathbf{R}_I\}$ ($I=1,2$ for dimers) specifies the potential $\hat{V}$ in which the electrons adjust in order to minimize the total energy of the system. The ground-state energy $E[\rho]$ of N electrons in the external potential $\hat{V}$ is given by Refs. 1, 2, and 5 (atomic Hartree units are used throughout the paper):

$$E[\rho]=\sum_i f_i\langle\psi_i|-\tfrac{1}{2}\nabla_i^2+\tfrac{1}{2}V_H+\varepsilon_{\rm XC}+\hat{V}|\psi_i\rangle + E_{\text{ion-ion}} , \tag{1}$$

where ρ is the electron density,

$$\rho(\mathbf{r})=\sum_i f_i|\psi_i(\mathbf{r})|^2 . \tag{2}$$

The sums extend over the occupied independent-particle orbitals $\{\psi_i\}$ whose occupation numbers are f_i. As described in detail below, we include explicitly in the computation only the valence electrons of the system. V_H is the Hartree potential

$$V_H(\mathbf{r})=\int\frac{\rho(\mathbf{r}')d\mathbf{r}'}{|\mathbf{r}-\mathbf{r}'|} . \tag{3}$$

$\varepsilon_{\rm XC}$ is the exchange and correlation potential in the LDA.[11] $E_{\text{ion-ion}}$ is a purely classical term describing the direct ion-ion interaction. $\hat{V}$ is the sum of ionic pseudopotentials:

$$\hat{V}(\mathbf{r})=\sum_I\hat{v}_{\rm ps}(\mathbf{r}-\mathbf{R}_I) , \tag{4}$$

where $\hat{v}_{\rm ps}$ is given by

$$\hat{v}_{\rm ps}=\sum_{l=0}^{\infty}v_l(r)\hat{P}_l . \tag{5}$$

$\hat{P}_l$ is the projection operator onto the lth angular momentum. $\hat{v}_{\rm ps}$ is a nonlocal operator since it acts differently on different angular components of the single-particle orbitals. The pseudopotentials v_l are obtained from first-principles relativistic atomic computation.[12] This enables us to take into account scalar relativistic effects.[13] Here, potentials for $l>2$ have been assumed to be equal to v_2; the explicit form used for $\hat{v}_{\rm ps}$ is

$$\hat{v}_{\rm ps}(\mathbf{r})=v_{\rm local}(r)+\Delta v_0\hat{P}_0+\Delta v_1\hat{P}_1 . \tag{6}$$

$v_{\rm local}=v_2$; Δv_l are short-range terms given by the difference (v_l-v_2), which have been fitted by a small set of Gaussian-type functions [$\exp(-a_ir^2)$ and $r^2\exp(-a_ir^2)$, $i=1,3$].[14] For a given ionic configuration $\{\mathbf{R}_I\}$ and number of electrons N, the orbitals $\{\psi_i\}$ minimizing $E[\rho]$ are eigenstates of the Kohn-Sham (KS) one-particle Hamiltonian $\hat{H}$,

$$\hat{H}\psi_i=\varepsilon_i\psi_i , \tag{7}$$

where

$$\hat{H}=-\tfrac{1}{2}\nabla^2+V_H+\mu_{\rm XC}+\hat{V} \tag{8}$$

and

$$\mu_{\rm XC}=\partial(\rho\varepsilon_{\rm XC})/\partial\rho . \tag{9}$$

For homonuclear dimers $\hat{H}$ has $D_{\infty h}$ symmetry and the orbitals may be chosen to be eigenstates of rotations around the z axis of the molecule and parity with respect to the plane $z=0$ (see Fig. 1).

Therefore, we can write

$$\psi_i(\mathbf{r})=e^{\pm im\varphi}\phi_i(r,z) , \tag{10}$$

where (r,z) are cylindrical coordinates and m is the azimuthal quantum number of the orbital ψ_i. The ϕ_i are either even or odd functions of z. We impose the boundary

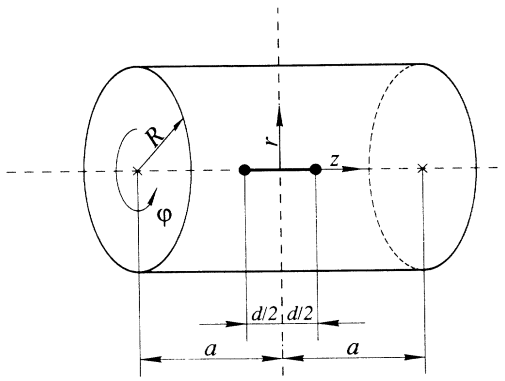

FIG. 1. Geometry of the unit cell used in the present computation. The cell is periodically repeated in the z direction.

conditions for ϕ_i at the surface of a cylinder of radius R and height $2a$ surrounding the molecules, as illustrated in Fig. 1. In the z direction we require the periodic boundary conditions

$$\phi_i(r,-a+z)=\phi_i(r,a+z), \quad r\leq R \tag{11}$$

to be satisfied, while on the lateral surface of the cylinder we impose

$$\phi_i(R,z)=0, \quad -a<z\leq a \ . \tag{12}$$

In this geometry the set of functions

$$\{e^{iG_z z}J_m(G_r r)\} \tag{13}$$

(where J_m is the Bessel function of the first kind of order m) is a complete basis set satisfying the above boundary conditions provided that

$$G_z=\frac{\pi}{a}n, \quad n=0,\pm1,\pm2,\ldots \tag{14}$$

and

$$G_r=\frac{\mu_l}{R}, \quad l=1,2,\ldots . \tag{15}$$

$\{\mu_l\}$ are the zeros of J_m.[15] We can therefore expand the orbitals ϕ_i as

$$\phi_i(r,z)=\sum_{G_r}\sum_{G_z} C_i(G_r,G_z)e^{iG_z z}J_m(G_r r) \ . \tag{16}$$

The coefficients $C_i(G_r,G_z)$ are given by the Fourier-Bessel formula

$$C_i(G_r,G_z)=\frac{1}{aR^2J_{m+1}^2(G_r R)}\int_{-a}^{+a}e^{iG_z z}dz \times\int_0^R rJ_m(G_r r)\phi(r,z)dr \ . \tag{17}$$

In a similar fashion all the other quantities entering the computation [such as the density ρ, the Coulomb potential $V_H(\mathbf{r})$, and the local part of the pseudopotential $V_{\rm loc}$] are expanded into Fourier-Bessel components. Substitution of Eq. (15) into (1) gives the expression for the total energy $E[\rho]$ as a function of the $\{C_i\}$. The kinetic energy ($E_{\rm kin}$) is easily written as an explicit function of these coefficients:

$$E_{\rm kin}=\pi aR^2\sum_i f_i\sum_{G_r}\sum_{G_z}J_{m+1}^2(G_r R)(G_r^2+G_z^2) \times|C_i(G_r,G_z)|^2 \ . \tag{18}$$

Other contributions to $E[\rho]$ (Hartree, local part of the pseudopotential energy, and exchange-correlation energy) are expressed as functions of the density ρ:

$$E_H=\tfrac{1}{2}\int\int\frac{\rho(\mathbf{r}')\rho(\mathbf{r})d\mathbf{r}\,d\mathbf{r}'}{|\mathbf{r}-\mathbf{r}'|} \ , \tag{19}$$

$$E_{\rm local}=\int V_{\rm local}(\mathbf{r})\rho(\mathbf{r})d\mathbf{r} \ , \tag{20}$$

$$E_{\rm XC}=\int\varepsilon_{\rm XC}(\rho(\mathbf{r}))\rho(\mathbf{r})d\mathbf{r} \ , \tag{21}$$

and their implicit dependence on the $\{C_l\}$ is established via Eqs. (2) and (16). Special problems are posed by the nonlocal part of the pseudopotential energy ($E_{\rm nonlocal}$). The computation of this term is discussed in the Appendix.

The traditional approach to minimization of total energies with respect to the $\{C_i\}$ is via the KS equations[2] and requires the diagonalization of the Hamiltonian matrix

$$(\hat{H})=\langle G_r,G_z,m|\hat{H}|G_r',G_z',m\rangle \ .$$

As is well known,[16,3] the diagonalization step must be repeated many times in order to achieve self-consistency between the charge density and the operator $\hat{H}$.

Here we take a very different approach. As suggested in Ref. 9 and used in several computations,[17] we evaluate the gradient of $E[\rho]$ with respect to the coefficients $\{C_l^*\}$. Then, starting from a given Fourier-Bessel decomposition for the $\{\psi_l\}$, we minimize the energy by using the information contained in $\partial E/\partial C_i^*$.

The gradient of $E_{\rm kin}$ with respect to the $\{C_i^*\}$ is

$$\frac{\partial E_{\rm kin}}{\partial C_i^*(G_r,C_z)}=\pi aR^2J_{m+1}^2(G_r R)(G_r^2+G_z^2)C_i(G_r,G_z) \ . \tag{22}$$

The computation of the gradients of E_H, $E_{\rm local}$, and $E_{\rm XC}$ involves an additional step. For $E_{\rm local}$ we have

$$\frac{\partial E_{\rm local}}{\partial C_l^*(G_r,G_z)}=\frac{\partial}{\partial C_l^*(G_r,G_z)}\times\sum_j\int d\mathbf{r}\,V_{\rm local}(\mathbf{r})\psi_j(\mathbf{r})\psi_j^*(\mathbf{r}) =\int d\mathbf{r}\,V_{\rm local}(\mathbf{r})\psi_i(\mathbf{r})e^{-iG_z z}J_m(G_r r) \ . \tag{23}$$

Similarly, for E_H and $E_{\rm XC}$ we obtain

$$\frac{\partial E_H}{\partial C_i^*(G_r,G_z)}=\int d\mathbf{r}\,\psi_i(\mathbf{r})e^{-iG_z z}J_m(G_r r)\int\frac{\rho(\mathbf{r}')d\mathbf{r}'}{|\mathbf{r}-\mathbf{r}'|} \ , \tag{24}$$

$$\frac{\partial E_{\rm XC}}{\partial C_i^*(G_r,G_z)} = \int d\mathbf{r}\,\psi_i(\mathbf{r}) e^{-iG_z z} J_m(G_r r)\mu_{\rm XC}(\mathbf{r}) \ . \tag{25}$$

The comparison of Eqs. (23)–(25) with Eq. (17) shows that (apart from trivial factors) the gradient of an energy term of the form $\int F(\mathbf{r})\rho(\mathbf{r})d\mathbf{r}$ is given by the Fourier-Bessel transform of the product $F(\mathbf{r})\psi(\mathbf{r})$. The gradient of $E_{\rm nonloc}$ is discussed in the Appendix.

Some of the advantages of this approach are apparent.

(i) It does not require the evaluation and storage of the full matrix $\hat{H}$.

(ii) It avoids Hamiltonian matrix diagonalization, which is computationally very expensive: Indeed the number of operations grows as the cube of the number of basis functions included in the computation.

(iii) Once the total energy has been minimized for a given ionic configuration $\{\mathbf{R}_I\}$, it is straightforward to update the solution for new (not very different) ionic positions. Furthermore, the calculation can be started with a small basis set and then the solution improved, by adding basis functions.

Prerequisites for this scheme to be competitive compared with approaches based on matrix diagonalization are (i) an efficient evaluation of $E(\{C_i\})$ and $\partial E[\rho]/\partial C_i^*(G_r,G_z)$, and (ii) an efficient minimization algorithm able to drive the system to the ground state in the smallest possible number of iterations.

III. COMPUTATIONAL CONSIDERATIONS

The basis set specified by Eq. (13) is reduced to a finite set by including in the computation only the functions with kinetic energy (ek) smaller than a given cutoff energy $E_{\rm cut}$:

$$ek = \tfrac{1}{2}(G_r^2+G_z^2) < E_{\rm cut} \ . \tag{26}$$

It is easy to verify that the number of basis functions satisfying Eq.(26) grows linearly with $E_{\rm cut}$.

The implementation of the scheme outlined in Sec. II requires, first of all, an efficient algorithm to transform between real and reciprocal space. The transform between the (z,G_z) variables is a usual Fourier transform. It is handled by a standard fast Fourier (FF) routine and does not need to be discussed here. The numerical transformation between the (r,G_r) variables has been discussed in detail by Lado.[18] We follow closely his prescriptions for its implementation. The $\{G_r\}$ grid [Eq. (15)] implicitly defines a discrete grid in real space:

$$r_i = \frac{\mu_i R}{\mu_{N_r}}, \quad i=1,2,\ldots,N_r \ . \tag{27}$$

N_r is the number of points of both $\{G_r\}$ and r grids. The discretized form of Eq. (17) is

$$C_i(G_r,G_z) = \frac{1}{N_z} W_+(G_r) \sum_{j=1}^{N_z}\sum_{k=1}^{N_r} e^{-iG_z z_j} \times W_-(r_k) r_k J_m(G_r r_k) \times \phi_i(r_k,z_j) \ . \tag{28}$$

N_z is the number of points in the (z,N_z) grid and the weight functions W_+ and W_- are chosen so that the orthogonality relations between Bessel functions are satisfied (see Ref. 18 for details):

$$W_+(G_r) = \frac{2}{R^2 G_r [J_{m+1}(G_r R)]^2} \ , \tag{29}$$

$$W_-(r_i) = \frac{2}{G_{N_r}^2 r_i [J_{m+1}(G_{N_r} r_i)]^2} \ . \tag{30}$$

We note that functions corresponding to different m are tabulated on different grids both in real and reciprocal space. When needed, functions of a given m can be computed from the tabulated ones, by interpolation.

The number of operations required by the transform (28) or its inverse (16) grows like N_r^2. N_z of such transforms are needed to obtain the two-dimensional (2D) array $\phi(r,G_z)$ from $\phi(G_r,G_z)$ (or vice versa). Therefore, the number of operations required by this step of the computation is of order of $N_z N_r^2$.

The transform of the (z,G_z) variables is less demanding. From well-known results of computational analysis (see, for instance, Ref. 19), we estimate it to require $\simeq N_r N_z \ln N_z$ operations.

If we define $N_{\rm tot} \cong N_r N_z$ and assume $N_r \cong N_z$, we obtain that for large $N_{\rm tot}$ the time needed for Fourier-Bessel transforms (FBT) grows like $N_{\rm tot}^{3/2}$. This scaling law is less favorable than that of the FF algorithm, adopted in most three-dimensional (3D) computations using plane-wave basis sets. However, the advantages of the 2D formulation are not offset by the worst asymptotic behavior of the FBT transform, in the range of $N_{\rm tot}$ attainable in practical computations.

The basic steps involved in the computation of $E[\rho]$

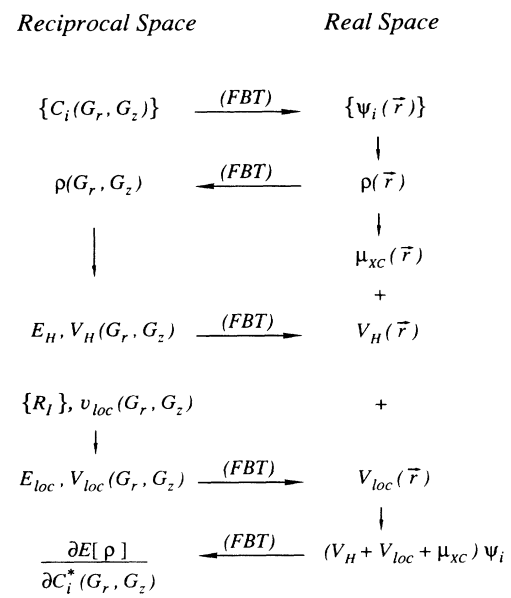

FIG. 2. Block diagram illustrating the basic steps making up one iteration in the computation of the total energy. FBT indicates a direct ($\rightarrow$) or inverse ($\leftarrow$) Fourier-Bessel transform. See text for the definition of the various quantities.

and $\partial E/\partial C_i^*$ are illustrated in Fig. 2; this shows the most convenient space (real or Fourier space) chosen for the evaluation of different terms, and the number of FBT transforms needed in our calculation.

In the framework of the Car-Parrinello method, a variety of algorithms have been proposed, which make use of the gradient $\partial E/\partial C_i^*$ in order to reach the minimum of $E[\rho]$.[20–22]

The simplest choice is to move the $\{C_i\}$ in the direction opposite to the gradient, following a steepest descent path. According to the formulation in the terms of "equations of motion" introduced in Ref. 9, this corresponds to

$$\dot{C}_i(G_x,G_z)=-\frac{\partial}{\partial C_i^*(G_x,G_z)}(E[\rho]-\varepsilon_i\langle\psi_i|\psi_i\rangle)\ . \qquad (31)$$

The $\{\varepsilon_i\}$ are Lagrange multipliers that ensure the orthonormality of the orbitals.

This simple algorithm has been used for part of the computations presented here. However, it is not very efficient, since it requires a very large number of iterations ($\sim$2000) for $E[\rho]$ to converge to its minimum.

A major improvement is offered by a minimization scheme based on the conjugate gradient algorithm,[19] which reduces the number of iterations by a factor of 10. Our implementation follows closely the one suggested by Štich *et al.*[22] Most of the results presented here have been obtained with this technique.

IV. RESULTS: THE IB DIMERS

The chemistry of molecules containing transition-metal atoms has recently been the subject of extensive *ab initio* investigations. In what follows we only refer to those works directly related to our computation; exhaustive reviews can be found in Refs. 23 and 24.

Among the three IB homonuclear dimers, Cu_2 is the most extensively studied both experimentally and theoretically. In recent LDA computations[25] its equilibrium distance has been found to be 4.18 a.u., in excellent agreement with the experimental value of 4.1947 a.u.[26] Less impressive, but still very good, is the agreement with experiment obtained for the binding energy D_e and vibrational frequency ω_e. DFT-LDA results for Ag_2 are reported in Refs. 27 and 28. Both computations have been performed within the pseudopotential approximation and rely on an expansion of the KS orbitals in a Gaussian basis set. As for Cu_2, the comparison between computed and measured quantities is good, especially so for r_e.

All-electron relativistic computations for Au_2 have been carried out by Ziegler *et al.*[29] Molecular orbitals were expanded in a small set of localized (Slater-type) basis functions and the exchange-correlation energy treated in the $X\alpha$ approximation. Again, the computed values for D_e, r_e, and ω_e are in good agreement with the experimental data.

Neutral and ionized group IB dimers have been extensively studied with SCF-HF or CI techniques (see Ref. 24 for a recent review). As far as the ground-state properties are concerned, the agreement with experiment is in general poorer than that obtained within LDA.

In the present computation Cu, Ag, and Au are described by a pseudopotential model in which the valence charge is given by the $nd^{10}(n+1)s^1$ atomic electrons (n=3,4,5 for Cu, Ag, and Au, respectively). All pseudopotentials are of the Hamann, Schlüter, and Chiang type.[12] For Ag and Au we used the tabulation of Ref. 14, whereas for Cu we generated a smoother pseudopotential.[30] Notwithstanding our modification, the d component of the Cu pseudopotential is much deeper and sharper than that of Ag or Au. This results in a higher kinetic energy cutoff ($E_{\rm cut}$) needed to achieve convergence with respect to the basis functions for Cu (and Zn), compared to Ag and Au (or Cd and Hg; see Table I). The convergence of the total energy and eigenvalues of an Ag atom as a function of $E_{\rm cut}$ is plotted in Fig. 3. This behavior is representative also for Au, Cd, and Hg, whereas for Cu and Zn the convergence is slower. However, the energies of interest [such as the potential energy $E(r)$, the bond energy D_e, etc.] are defined as differences of total energies and these are known to converge faster than total energies themselves. Indeed, plots of $E(r)$ computed for different $E_{\rm cut}$ (see Fig. 4 for a representative example) show that energy differences are close to convergence at cutoffs significantly smaller than those used in our computation. The global accuracy (i.e., including basis-function convergence and numerical accuracy) of our curves is estimated to be of the order of a few 0.01 eV for the neutral dimers. As discussed below, the

TABLE I. Dimension a and R of the unit cell and degree of convergence of the atomic total energy $E_{\rm tot}$, valence eigenvalues $\varepsilon_d,\varepsilon_s$ at the cutoff energy $E_{\rm cut}$ used in the present computation for the IB and IIB elements. $\Delta E_{\rm tot}$, $\Delta\varepsilon_d$, $\Delta\varepsilon_s$ are defined as $E_{\rm tot}(E_{\rm cut})-E_{\rm tot}(\infty)$, $\varepsilon_d(E_{\rm cut})-\varepsilon_d(\infty)$, $\varepsilon_s(E_{\rm cut})-\varepsilon_s(\infty)$, respectively. The reference values $E_{\rm tot}(\infty)$, $\varepsilon_d(\infty)$, $\varepsilon_s(\infty)$ are given by an atomic computation in spherical geometry on a logarithmic mesh.

Element	$a=R$ (a.u.)	$E_{\rm cut}$ (Ry)	$\Delta E_{\rm tot}$ (hartree)	$\Delta\varepsilon_d$ (hartree)	$\Delta\varepsilon_s$ (hartree)
Cu	11.5	306	0.018	-5×10^{-4}	-4×10^{-4}
Ag	12.0	70	0.024	-4×10^{-4}	-6×10^{-6}
Au	14.0	52	0.010	-8×10^{-5}	-1×10^{-4}
Zn	11.5	306	0.047	-7×10^{-4}	-9×10^{-5}
Cd	12.0	70	0.036	-8×10^{-4}	-9×10^{-5}
Hg	14.0	52	0.013	-3×10^{-4}	-1×10^{-4}

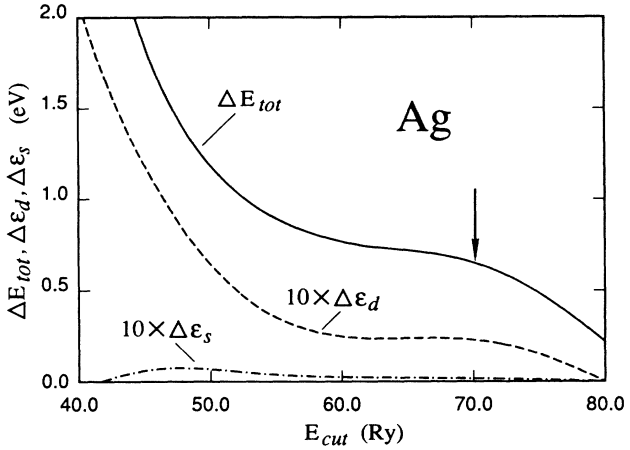

FIG. 3. Convergence of the total energy $E_{\rm tot}$ and valence eigenvalues $\varepsilon_d, \varepsilon_s$ of a silver atom as a function of the kinetic-energy cutoff $E_{\rm cut}$. The asymptotic values $E_{\rm tot}(\infty)$, $\varepsilon_d(\infty)$, $\varepsilon_s(\infty)$ are provided by an atomic computation in spherical geometry on a logarithmic mesh. The arrow indicates the cutoff $E_{\rm cut}$ used in our computation.

estimate is less favorable for ionized systems.

The potential-energy curves $E(r)$ for Cu_2, Ag_2, and Au_2 are displayed in Fig. 5. Over the full range of the plot they are fitted with an error of less than 2×10^{-2} eV by the modified Morse potential of Hulburt and Hirschfelder[31] (HH):

$$E(r)=D_e[(1-e^{-\beta x})^2+b\beta^3x^3e^{-2\beta x}(1+a\beta x)-1]\ , \quad (32)$$

where $x=r-r_e$. The values of the fitting parameters are reported in Table II, where we also compare the computed spectroscopic constants to the availale experimental data. The LDA calculations reproduce correctly all the trends observed experimentally. As expected, the computed r_e is very close to the measured value; ω_e, although overestimated, is within 10% of the experimental results. The cohesive energy D_e, instead, is largely overestimated,

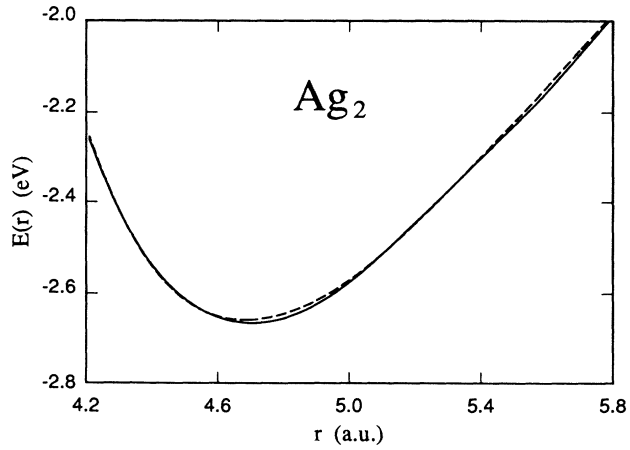

FIG. 4. Potential-energy curve $E(r)$ of Ag_2 computed at two different cutoffs $E_{\rm cut}$. Solid line, $E_{\rm cut}=70$ Ry; dashed line, $E_{\rm cut}=60$ Ry.

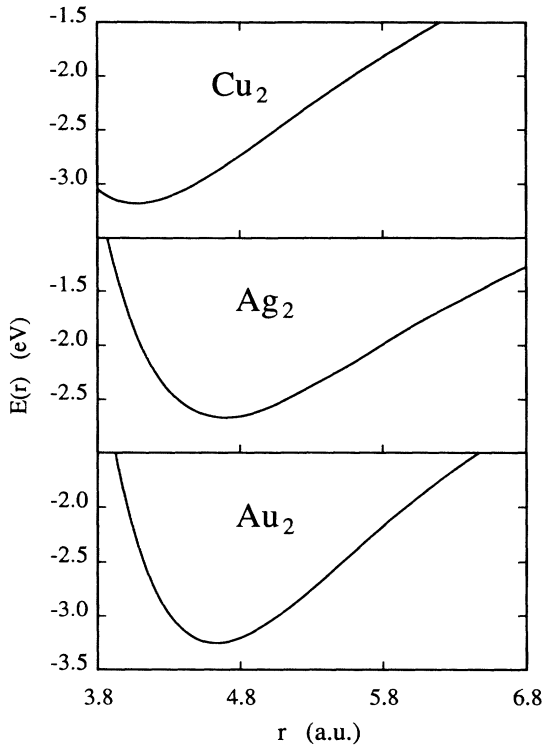

FIG. 5. Potential-energy curves $E(r)$ for Cu_2, Ag_2, and Au_2.

the error being of 61% for Cu_2 and Ag_2, 41% for Au_2. The spin unpolarized approximation is responsible only in part for this discrepancy. Indeed, we find that the local-spin-density total energy of two isolated atoms differs from the LDA value by 0.38, 0.31, and 0.27 eV for Cu, Ag, and Au, respectively, thus accounting for only about one-third of the error.

Of particular interest is the comparison with the theoretical values obtined for Ag_2 in Ref. 28(a). Since the authors used the same pseudopotential and exchange-correlation approximation as those adopted here, discrepancies between their and our findings must be attributed to the different basis set adopted for the expansion of the KS orbitals. The differences found for r_e and D_e (4.75 a.u. and 2.5 eV reported in Ref. 28, to be compared with our results of 4.69 a.u. and 2.67 eV, respectively) are consistent with the improved completeness of the basis set used in the present computation.

Similarly, for Cu_2 and Au_2 we compute cohesive energies significantly larger than those reported in Refs. 25 and 29. However, in this case part of the discrepancy is due to the different physical model used in our calculation.

Ionized dimers pose special problems, which arise from the periodicity of the charge in the z direction, implicit in the expansion (16). Although the net charge is easily neutralized by a uniform background, the interaction of higher multipoles in the periodic replicas can be non-negligible and decays very slowly with the size of the unit cell.

We performed computations for Ag_2^+ and Au_2^+ in a unit cell of side (R and a) double that listed in Table I for

TABLE II. Bonding parameters for the neutral dimers: bonding length r_e, cohesive energy D_e, vibrational frequency ω_e. See text, Eq. (31), for the definitions of β, a, and b. r_e, D_e, β, a, and b are obtained by a mean-square fit of the HH curves to the numerical results. Numbers in parentheses give the experimental values (the data for Zn_2 and Cd_2 are from Ref. 39, for Hg_2 from Ref. 40; all the other experimental results are from Ref. 26).

Dimer	r_e (a.u.)	D_e (eV)	β (a.u.$^{-1}$)	a	b	ω_e (cm^{-1})
Cu_2	4.07	3.18	0.669	0.283	−0.209	295.1
	(4.195)	(1.97)				(264.5)
Ag_2	4.69	2.67	0.671	0.731	−0.156	207.3
	(4.67)	(1.66)				(192.4)
Au_2	4.63	3.25	0.766	1.250	−0.071	193.2
	(4.67)	(2.30)				(191.0)
Zn_2	5.29	0.23	0.669	−1.017	−0.206	78
	(7.56)	(0.06)				
Cd_2	5.77	0.24	0.742	0.207	−0.098	67
	(9.10)	(0.05)				
Hg_2	5.65	0.23	1.069	0.488	0.263	71
	(6.86)	(0.07)				

the neutral systems. The self-consistent charge density was then transferred in a larger box ($R=a=48$ and 56 a.u., corresponding to volumes of 7×10^5 and 1.1×10^6 a.u.^{3} for Ag and Au, respectively), in order to recompute the electrostatic energy, without, however, reoptimizing the wave functions. The results are collected in Fig. 6 and Table III.

Despite the very large volume of the unit cell, we still expect a sizable effect of the interaction among periodic replicas. In order to estimate its magnitude, we have compared the ionization potential of a single atom, as computed with our technique, to that obtained with atomic calculations in spherical geometry and with the proper boundary conditions. The two values differ by 0.15–0.20 eV at most: This can be taken as an estimate of the accuracy of the computed ionization potentials. The error should be much smaller for the potential-energy curves $E(r)$. These are defined as energy differences between equally ionized configurations and their interaction with distant replicas is effectively subtracted out.

We notice that the experimental dissociation limit of the ionized dimers ($A_2^+ \rightarrow A + A^+$) is not correctly reproduced by LDA. Indeed, for large internuclear separations, we still find symmetric distribution of the charge on the two monomers. Therefore, the dissociation energy for the ionized species is computed with respect to the sum of the energies of A and A^+ obtained in two different computations.

Due to the large size of the computation, we did not include spin polarization effects nor did we investigate Cu_2^+. Unfortunately, the available experimental information for Ag_2^+ and Au_2^+ is very limited and the ionization energies of Ag_2 and Au_2 have not yet been measured.

Our results show a qualitative difference between silver and gold dimers that might be related to the experimental detection of Au^{2+} recently reportecd by Ref. 7. The vari-

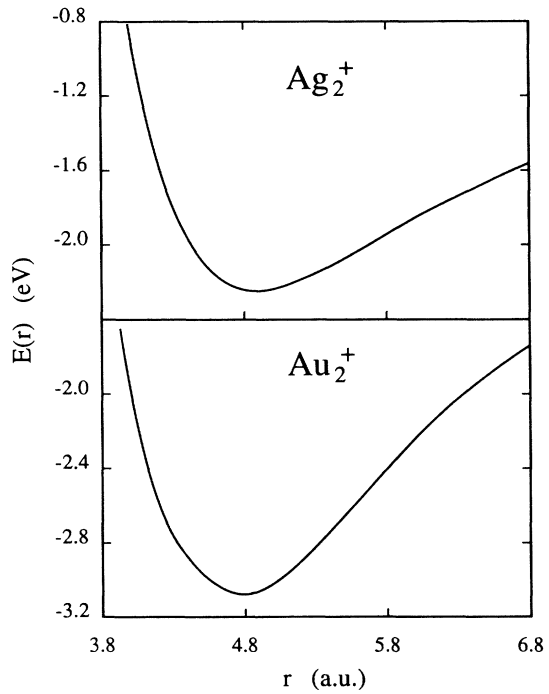

FIG. 6. Potential-energy curves $E(r)$ for Ag_2^+ and Au_2^+. See text for the definition of the zero of $E(r)$.

TABLE III. Vertical (VIP) and adiabatic (AIP) ionization potential of Ag_2, Au_2, Cd_2, and Hg_2. Bonding length r_e, cohesive energy D_e, and vibrational frequency ω_e of the ionized dimers. Numbers in parentheses give the experimental values.

Dimer	VIP (eV)	AIP (eV)	r_e (a.u.)	D_e (eV)	ω_e (cm^{-1})
Ag_2^+	8.34	8.31	4.89	2.24	161.1
Au_2^+	9.75	9.71	4.77	3.07	157.0
Cd_2^+	7.67	7.60	5.21	2.05	125.1
Hg_2^+	8.95	8.74	5.08	2.20	126.3
	(9.10)			(1.40)	

ational principle stated by Eq. (1) implies a minimization with respect to both $\{C_i\}$ *and* the occupation numbers $\{f_i\}$. Minimization with respect to $\{f_i\}$ is easily attainable for Ag_2^+. For each distance, the occupied orbital of highest energy is the σ bonding state, coming from the atomic 4*s* levels. The energy minimum for Ag_2^+ corresponds to the removal of one of these two bonding electrons; this results in an increase of r_e ($\Delta r_e = 0.20$ a.u.) and a decrease of D_e ($\Delta D_e = 0.43$ a.u.) with respect to the neutral dimer.

The situation is more complicated for gold. The bonding character of the highest occupied molecular orbital (HOMO) depends upon distance: The HOMO is a σ bonding state for $r \geq 4.8$ a.u., and a σ^* antibonding state, given by the 5*d* atomic orbitals, for $r \leq 4.2$ a.u. Therefore, the energy minimum corresponds to the removal of a bonding electron at long distances ($r \geq 4.8$ a.u.) and of an antibonding one at short distances ($r \leq 4.2$ a.u.). For intermediate bond lengths, the energy is minimized by fractional occupation numbers, corresponding to degenerate σ and σ^* levels. The partial removal of an antibonding electron for distances close to r_e makes Au_2^+ to be only 0.18 eV less bonded than Au_2, and its equilibrium distance slightly longer ($\Delta r_e = 0.14$ a.u.). The stability of Au_2^+ might be related to the experimental observation of Au_2^{2+}. Its existence, even as a metastable species, requires strong short-range bonding forces to be still present, in order to balance the Coulomb repulsion of the two positive charges. According to this picture, Ag_2^{2+} should not be observed. In this case, the removal of the second σ electron leaves behind two closed-shell ions that will repeal each other for each distance. Calculations are in progress to substantiate this speculation.

V. RESULTS: THE IIB DIMERS

A few years ago, the suggestion that Group IIB dimers could act as active media for excimer lasers[32] has motivated a surge of interest in the physical properties of these molecules. More recently, the interest has been renewed by the observation of a nonmetal-to-metal transition in small mercury aggregates.[33] A similar transition, not yet observed, may be expected also for Zn and Cd clusters.

The dimers of Group IIB exhibit characteristics remarkably different from those of Group IB; a similar diversity of physical properties is observed between alkali and alkali-earth metals. The two additional valence electrons in the filled $ns^2 (n=4,5,6)$ atomic states occupy an antibonding molecular orbital: This reduces drastically the cohesive energy of the IIB dimers, with respect to the IB molecules. The limited stability of Zn_2, Cd_2, and Hg_2 is responsible for large uncertainties in the experimental values of their D_e, r_e, and ω_e. (Here we adopt as our main reference the values tabulated by Huber and Herzberg,[26] although more recent measurements are available for some of these molecules.) An increase in bond energy (with respect to the dissociation products) may be obtained either by ionization[34] or excitation.[35]

No systematic investigation of Zn_2, Cd_2, or Hg_2 has been carried out in DFT-LDA,[36] whereas these dimers have been extensively studied with SCF-HF or CI techniques. However, most of these computations predicted for the ground state a purely repulsive potential-energy curve.

In Ref. 8 we reported the results of a detailed study of Hg_2 and Hg_2^+. Here we extend our investigation to dimers of zinc and cadmium. The 12 electrons of the $nd^{10}(n+1)s^2$ atomic levels have been included in the valence charge. The pseudopotentials for Cd and Hg are from Ref. 14, while we generated a softer pseudopotential for zinc.[30] Only the neutral Zn dimers has been investigated, for the same reasons already discussed for Cu (see Sec. IV). The size of the unit cell used in the computation, together with the parameters specifying the convergence of E_{tot} with respect to E_{cut} are reported in Table I. $E(r)$ for Zn_2, Cd_2, and Hg_2 are plotted in Fig. 7. Again, the HH curve fits very well the numerical results over a large interval of interatomic distances. The five parameters of the fit are listed in Table II. The properties of Cd_2^+ and Hg_2^+ have been computed following the procedure described in Sec. IV; our results are collected in Fig. 8 and Table III.

Although LDA correctly reproduces several qualitative properties of the Group IIB molecules—such as those of weakly bonded systems, with similar bonding parameters and large excitation energies—significant discrepancies with experiment are found by our calculations. The errors on the equilibrium distances and vibrational frequencies are much larger than those observed in more stable molecules, and the bond energies of all the dimers are greatly overestimated. The large relative errors for the neutral systems, however, are also due to the very

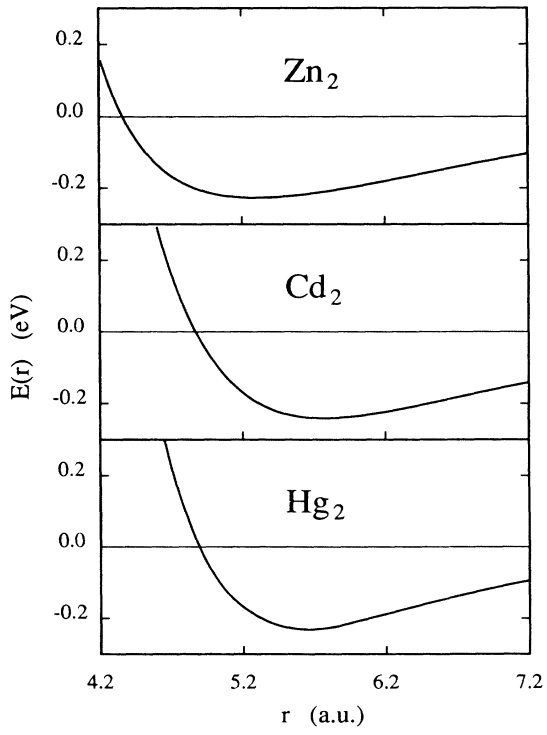

FIG. 7. Potential-energy curves $E(r)$ for Zn_2, Cd_2, and Hg_2.

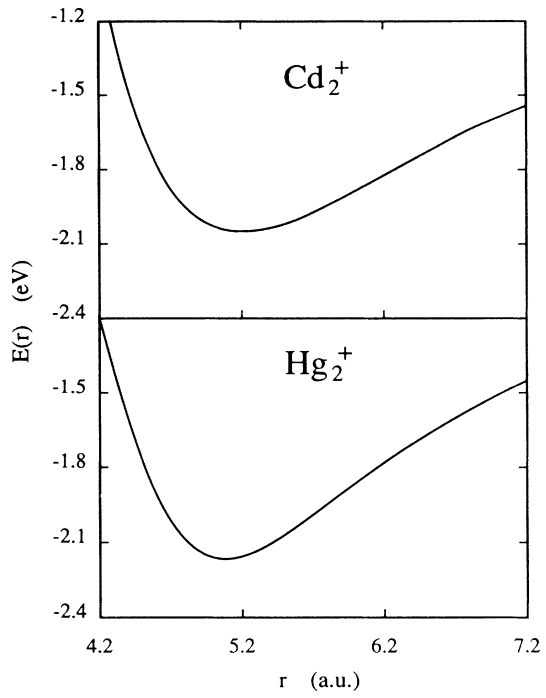

FIG. 8. Potential-energy curves $E(r)$ for Cd_2^+ and Hg_2^+. See text for the definition of the zero of $E(r)$.

small absolute values of the experimental cohesive energies. An all-electron full-potential computation[37] showed that the discrepancies with experiment are not an artifact of the pseudopotential model. Instead, they must be attributed to the inadequacy of LDA in describing the delicate energy balance of these very weak bonds.

In the Group IB atoms the uppermost d level and the s valence state are so close in energy and spatial extent ($\varepsilon_d - \varepsilon_s = 0.49$, 2.98, and 1.12 eV for Cu, Ag, and Au, respectively) to make unambiguous their participation to the chemistry of these elements. For the group IIB, the definition of their valence charge is less clear. The d and s states still occupy the same region of space. However, the difference of their eigenvalues is somewhat larger ($\varepsilon_s - \varepsilon_d = 4.23$, 5.98, and 3.04 eV for Zn, Cd, and Hg, respectively) and it is reasonable to question the inclusion of the d electrons in the valence charge.

From a computational point of view, the possibility of freezing the d electrons in the core is particularly appealing. As already mentioned in Ref. 8, this simplification has two major beneficial consequences. First of all, it reduces the number of valence electrons by a factor of 6. More importantly, the potentials and charge densities relative to the s electrons are much smoother than those describing the highly localized d states. Therefore, the kinetic-energy cutoff $E_{\rm cut}$ required to achieve convergence is significantly reduced, thus implying a corresponding reduction of the number of basis functions in the expansion (16). As an additional advantage, a smaller $E_{\rm cut}$ usually corresponds to a faster convergence of the iterative procedure (either steepest descent or conjugate gradient) to the minimum of $E[\rho]$. For instance, we have verified that, including the d electrons in the core (see below for the description of the model we used), a satisfactory convergence for Zn_2, Cd_2, and Hg_2 is achieved with $E_{\rm cut}$ in the range 15–20 Ry. The number of conjugate gradient steps needed to minimize $E[\rho]$ as a function of the $\{C_i\}$ is reduced by a factor of 3–4 for Cd_2 and Hg_2, and by a factor of 10 for Zn_2. As a result, the time needed for the computation is reduced by nearly two orders of magnitude for Cd_2 and Hg_2, and by nearly three orders of magnitude for Zn_2.

However, in Ref. 8 we have shown that the repulsion between d states has to be properly included in the calculation, in order to account for the long interatomic distance of Hg_2. The same conclusion applies to Zn and Cd. Indeed, a computation in which only the $(n+1)s^2$ electrons are included in the valence (the pseudopotentials are from Table VI of Ref. 14) gives very short bond lengths ($R_e = 4.80$, 5.10, 4.63 a.u. for Zn_2, Cd_2, Hg_2) and large cohesive energies ($D_e = 0.33$, 0.45, 0.76 eV for Zn_2, Cd_2, Hg_2), in strong disagreement with both experiment and the full computation including d electrons in the valence charge. These results show the increasing strength of the d-d interaction, in going from Zn, where the d shell is very localized, to Cd and Hg.

The agreement between the simplified computation and the one including 12 valence electrons per atom is drastically improved, when corrections due to the nonlinearity in the exchange-correlation energy[10] are taken into account [$(n+1)s^2$+nonlinear core corrections (NLCC) model]. The bonding properties obtained in this way are listed in Table IV. The potential-energy curves agree very well with those of Fig. 7 for distances larger than the equilibrium distance. At shorter bond lengths the NLCC scheme is not sufficient to reproduce correctly the rise of the overlap repulsion (see Fig. 1 of Ref. 8 for an example).

The results of Table IV may lead one to think that the simple $(n+1)s^2$+NLCC scheme is even better than the full computation, when compared to the experimental data. However, the difference between the two sets of theoretical results is smaller than the uncertainties usually associated with different pseudopotential models. Moreover, the good result for ω_e obtained within he simpler model is partially due to the underestimation of the repulsive part of $E(r)$. Part of the difference in D_e and r_e may be systematic and could reflect the residual effect of the low-laying core states, somehow present in the $(n+1)s^2$+NLCC scheme but completely frozen in the $nd^{10}(n+1)s^2$ model.

As far as electronic properties are concerned, we find that the $(n+1)s^2$+NLCC scheme and the $nd^{10}(n+1)s^2$ computation give the same dependence upon interatomic distance, of the eigenvalues of the states coming from the

TABLE IV. Bonding parameters of Zn_2, Cd_2, and Hg_2 computed in the $(n+1)s^2$+NLCC pseudopotential scheme.

Dimer	$E_{\rm cut}$ (Ry)	r_e (a.u.)	D_e (eV)	ω_e (cm^{-1})
Zn_2	27.4	5.36	0.22	83.6
Cd_2	27.4	5.82	0.23	65.5
Hg_2	27.4	5.62	0.22	52.2

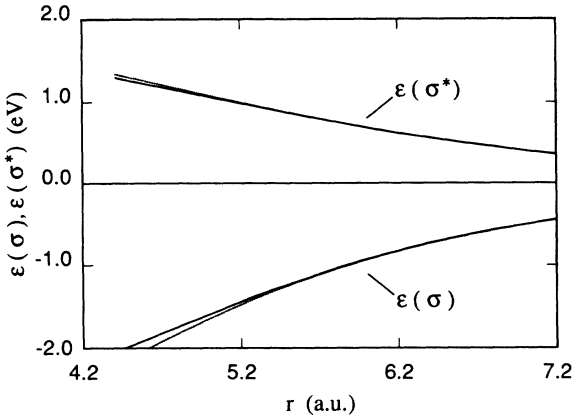

FIG. 9. Eigenvalues of the two highest occupied levels of Cd_2 as a function of interatomic distance. Solid line: results of the computation with 12 valence electrons per atom [$nd^{10}(n+1)s^2$ model]. Dashed line: results of the computation with two valence electrons per atom [$(n+1)s^2$+NLCC model]. The zero of the curves has been set equal to the eigenvalue of the 5*s* level of a cadmium atom.

atomic *s* levels (see Fig. 9). This suggests that the simpler scheme may provide a reliable model to study the electronic propeties of larger clusters. In particular, it may make possible the investigation of the nonmetal-to-metal transition as a function of size. However, in order to study structural and dynamical propeties of clusters, one should correct the expression of $E[\rho]$ to take into account the short-range repulsion due to the *d* shells. A simple and convenient recipe to include this contribution via a classical two-body potential has been proposed and tested for mercury in Ref. 8.

VI. CONCLUSIONS

We have presented a systematic investigation of the properties of neutral and ionized dimers of the IB and IIB groups in the pseudopotential local-density-approximation framework. We have assumed a valence charge configuration that includes the *d* and *s* atomic levels of highest energy. In order to approach the LDA limit with an accuracy of about 10^{-2} eV for the cohesive energy, we have expanded the single-particle orbitals in a large number of orthogonal basis functions, adapted to the symmetry of the Hamiltonian.

The total energy has been computed by minimizing the LDA energy functional via a technique derived from the Car-Parrinello method. Our scheme has several advantages over traditional techniques based on direct matrix diagonalization. Among them: It does not require the evaluation and storage of the full Hamiltonian matrix; the time spent for an iteration grows with the size of the basis set to the power $\frac{3}{2}$. This scaling law has to be compared with the well-known cubic dependence of the diagonalization procedure upon the number of basis functions.

The computed equilibrium distances of the IB neutral dimers are found to be in good agreement with both experimental data and previous computations. Our values for the cohesive energy are larger than those reported in previous studies. We find that LDA overestimates D_e of 61% for Cu_2 and Ag_2, and of 41% for Au_2.

The discrepancies between LDA and experimental data are larger for the IIB elements. The computed D_e is about 0.23 eV, whereas the experimental value is around 0.06 eV for all the IIB dimers. The equilibrium distances are underestimated by roughly 8–10%. However, LDA reproduces the qualitative features characterizing the bonding of these molecules. The neutral dimers are found to have very weak, though not van der Waals-like, bonds. Excited states are separated from the highest occupied level by 3.40 eV for Zn_2, 3.17 eV for Cd_2, and 4.50 eV for Hg_2. The ionized dimers have a cohesive energy of $\sim$2 eV, which is the usual strength of simple bonds. The computed vertical ionization energies go from 7.7 eV for Cd_2 to 9 eV for Hg_2.

In order to improve the quantitative agreement between computed and measured properties, work is in progress to include in our computations more refined approximations for the exchange and correlation energy.[5] Our scheme is easily adapted to each method preserving the independent-particle picture. The accuracy attainable by our algorithm may be important in discriminating unambiguously between different approximations.

A different development of our study points to the analysis of equilibrium geometries and electronic properties of larger clusters of Zn, Cd, and Hg. Such a project, which aims at the description of the van der Waals-to-metal transition observed for mercury cluster, should take advantage of the powerful *ab initio* molecular-dynamics technique, developed by Car and Parrinello. Our analysis of the role of the *d* electrons, carried out in Ref. 8 and in the present paper, may provide the crucial information needed to reduce the computational problem to manageable size.

ACKNOWLEDGMENTS

The authors would like to acknowledge useful discussions with G. Bachelet, R. Car, R. M. Martin, M. Parrinello, and R. Resta. This work has been supported by the Swiss National Science Foundation under Grant No. 20-5446.87 (P.B.) and by the National Science Foundation (NSF) under Grant No. DMR86-12860 (G.G.).

APPENDIX

Using the notation of Sec. II, the nonlocal contribution to the pseudopotential energy is written as

$$E_{\text{nonloc}} = \sum_{I}^{N_{\text{ions}}} \sum_{i} f_i \int d\mathbf{r}\, \psi_i^*(\mathbf{r}) \sum_{l=0}^{1} \Delta v_l(|\mathbf{r}-\mathbf{R}_I|) \times \hat{P}_l(\mathbf{R}_I)\psi_i(\mathbf{r}) , \quad \text{(A1)}$$

where $\Delta v_0, \Delta v_1$ are defined by Eqs. (5) and (6) and $\hat{P}_l(\mathbf{R}_i)$ are the projectors over the *l* angular momentum component of ψ_i around the ion at position $\mathbf{R}_I$.

The action of $\hat{P}_l$ may be made explicit by decomposing the ψ_i in angular components around each ion:

$$\psi_i(\mathbf{r})=\sum_{l,m}\frac{U_{lm}^{(i)}(|\mathbf{r}-\mathbf{R}_I|)}{|\mathbf{r}-\mathbf{R}_I|}Y_{lm}(\theta,\varphi|\mathbf{R}_I)\ , \tag{A2}$$

where $Y_{lm}(\theta,\varphi|\mathbf{R}_I)$ are spherical harmonics centered at $\mathbf{R}_I$. Then, E_{nonloc} may be written as

$$E_{\text{nonloc}}=\sum_I\sum_i f_i\sum_{l,m}\int_0^\infty dx|U_{lm}^{(i)}(x)|^2\Delta v_l(x)\ , \tag{A3}$$

where $x=|\mathbf{r}-\mathbf{R}_I|$.

Since Δv_l are Gaussian-type functions and the U_{lm} are short-range analytic functions, the integrals in (A3) are readily evaluated via a Gauss-Hermite integration formula:

$$E_{\text{nonloc}}=\frac{\alpha}{2}\sum_I\sum_i f_i\sum_{l,m}\sum_{n_{\text{IGH}}=1}^{n_{\text{NGH}}}W_{n_{\text{IGH}}}|U_{lm}^{(i)}(\alpha X_{n_{\text{IGH}}})|^2\times\Delta\tilde{v}_l(\alpha X_{n_{\text{IGH}}})\ . \tag{A4}$$

$X_{n_{\text{IGH}}}$ and $W_{n_{\text{IGH}}}$ are Gauss-Hermite integration points and weights, respectively, and n_{NGH} is the order of the integration formula. The $\Delta\tilde{v}_l$ are given by

$$\Delta\tilde{v}_l(x)=\exp(x/\alpha)^2\Delta v_l(x)\ , \tag{A5}$$

where α has been chosen in such a way that at infinity $\Delta\tilde{v}_l$ diverges not faster than a polynomial.

In the present computation n_{NGH} ranged from 40 (for Ag, Au, Cd, and Hg) to 80 (for Cu and Zn). The corresponding $\Delta\tilde{v}_l(\alpha X_{n_{\text{IGH}}})$ are easily computed and stored at the beginning of the iteration cycles. The crucial requirement for an efficient implementation of Eq. (A4) is a fast computation of the $U_{lm}^{(i)}(\alpha X_{n_{\text{IGH}}})$. Their explicit definition is

$$\frac{U_{lm}^{(i)}(X)}{X}=\int_0^{2\pi}d\varphi\int_0^\pi\sin\theta\,d\theta\,\psi_i(\mathbf{R}_I+\mathbf{X})Y_{lm}^*(\theta,\varphi|\mathbf{R}_I)\ , \tag{A6}$$

where, in spherical coordinates, $\mathbf{X}$ is the vector (X,θ,φ) describing a sphere of radius X around $\mathbf{R}_I$.

The integration in φ is immediately performed by taking into account the fact that each ψ_i has a well-defined azimuthal character $\bar{m}$. Then, we are left with the evaluation of a one-dimensional integral:

$$\frac{U_{lm}^{(i)}(X)}{X}=\delta_{m,\bar{m}}\int_0^\pi\sin\theta\,d\theta\,p_l(\cos\theta)\times\phi_i(X\sin\theta,R_I+X\cos\theta)\ , \tag{A7}$$

where $p_l(\cos\theta)$ are Legendre polynomials.

By a simple change of variable and by substituting the expansion (16) for ϕ_i, we finally arrive at

$$\frac{U_{lm}^{(i)}(X)}{X}=\delta_{m,\bar{m}}\sum_{G_r,G_z}C_i(G_r,G_z)e^{iG_zR_I}\times\int_{-1}^1 du\,p_l(u)e^{iG_zXu}\times J_m[G_rX(1-u^2)^{1/2}]\ . \tag{A8}$$

For $l=0,1$ integrals of this form are listed in Ref. 38. For instance, for $l=0$ we get

$$\frac{U_{00}^{(i)}(X)}{X}=\delta_{m,\bar{m}}2\sum_{G_r,G_z}C_i(G_r,G_z)e^{iG_zR_I}\times\frac{\sin[X(G_r^2+G_z^2)^{1/2}]}{[X(G_r^2+G_z^2)^{1/2}]}\ . \tag{A9}$$

From Eqs. (A4) and (A8) it is apparent that the number of operations required for the evaluation of E_{nonloc} grows linearly with the size of the basis set, in agreement with the findings of Ref. 22.

The same scaling law applies also to the computation of the gradient

$$\partial E_{\text{nonloc}}/\partial C_i^*(G_r,G_z)\ .$$

From Eq. (A4) we have

$$\frac{\partial E_{\text{nonloc}}}{\partial C_i^*(G_r,G_z)}=\alpha\sum_I\sum_i f_i\sum_{l,m}\sum_{n_{\text{IGH}}=1}^{n_{\text{IGH}}}W_{n_{\text{IGH}}}U_{lm}^{(i)}(\alpha X_{n_{\text{IGH}}})\times\frac{\partial U_{lm}^{(i)*}(\alpha X_{n_{\text{IGH}}})}{\partial C_i^*(G_r,G_z)}\times\Delta\tilde{v}_l(\alpha X_{n_{\text{IGH}}})$$

and $\partial U_{lm}^{(i)*}/\partial C_i^*(G_r,G_z)$ is readily obtained from Eq. (A8).

---

*Present address: Institut de Physique Expérimentale, Ecole Polytechnique Fédérale de Lausanne, PHB-Ecublens, 1015 Lausanne, Switzerland.

†Present address: IBM Research Division, Zurich Research Laboratory, CH-8803 Rüschlikon, Switzerland.

[1]P. Hohenberg and W. Khon, Phys. Rev. B **136**, 864 (1964).

[2]W. Kohn and L. J. Sham, Phys. Rev. **140**, A1133 (1965).

[3]G. P. Srivastava and D. Weaire, Adv. Phys. **36**, 463 (1987).

[4]R. O. Jones and O. Gunnarsson, Rev. Mod. Phys. **61**, 689 (1989).

[5]R. G. Parr and W. Yang, *Density Functional Theory of Atoms and Molecules* (Oxford University Press, Oxford, 1989).

[6]See, for instance, J. B. Danese, J. Chem. Phys. **61**, 3071 (1974); J. W. D. Connolly and J. R. Sabin, *ibid.* **56**, 5529 (1972).
[7]W. A. Saunders, Phys. Rev. Lett. **62**, 1037 (1989).
[8]P. Ballone and G. Galli, Phys. Rev. B **40**, 8563 (1989).
[9]R. Car and M. Parrinello, Phys. Rev. Lett. **55**, 2471 (1985).
[10]S. G. Louie, S. Froyen, and M. L. Cohen, Phys. Rev. B **26**, 1738 (1982).
[11]J. P. Perdew and A. Zunger, Phys. Rev. B **23**, 5048 (1981); D. M. Ceperley, *ibid.* **18**, 3126 (1978); D. M. Ceperley and B. J. Alder, Phys. Rev. Lett. **45**, 566 (1980).
[12]D. R. Hamann, M. Schlüter, and C. Chiang, Phys. Rev. Lett. **43**, 1494 (1979).
[13]L. Kleinman, Phys. Rev. B **21**, 2630 (1980).
[14]G. B. Bachelet, D. R. Hamann, and M. Schlüter, Phys. Rev. B **26**, 4199 (1982).
[15]G. N. Watson, *Theory of Bessel Functions,* 2nd ed. (Cambridge University Press, Cambridge, 1952).
[16]W. E. Pickett, Comput. Phys. Rep. **9**, 115 (1989).
[17]R. Car and M. Parrinello, in *Simple Molecular Systems at Very High Density,* Vol. 186 of *NATO Advanced Study Institute Series B: Physics,* edited by A. Polian, P. Loubeyre, and N. Boccara (Plenum, New York, 1989), and references therein.
[18]F. Lado, J. Comp. Phys. **8**, 417 (1971).
[19]W. M. Press, B. P. Flannery, S. A. Teukolsky, and W. T. Vetterling, *Numerical Recipes* (Cambridge University Press, Cambridge, 1986).
[20]M. C. Payne, J. D. Joannopoulos, D. C. Allan, M. P. Teter, and D. M. Vanderbilt, Phys. Rev. Lett. **56**, 2656 (1986).
[21]A. Williams and J. Soler, Bull. Am. Phys. Soc. **32**, 562 (1987).
[22]I. Štich, R. Car, M. Parrinello, and S. Baroni, Phys. Rev. B **39**, 4997 (1989).
[23]D. R. Salahub, in *Ab Initio Methods in Quantum Chemisty,* edited by K. P. Lawley (Wiley-Interscience, Chichester, 1987), Part II.
[24]*Comparison of Ab Initio Quantum Chemistry with Experiment for Small Molecules,* edited by R. J. Gartlett (Reidel, Dordrecht, 1985); C. W. Bauschlicher, Jr., S. R. Langhoff, and H. Partridge, J. Chem. Phys. **91**, 2412 (1989), and references therein.
[25]E. Radzio, J. Andzelm, and D. R. Salahub (unpublished). Report in Ref. 23.
[26]K. P. Huber and G. Herzberg, *Molecular Spectra and Molecular Structure. IV. Constants of Diatomic Molecules* (Van Nostrand, Princeton, 1979).
[27]J. Flad, G. Igel-Mann, H. Preuss, and H. Stoll, Ber. Bunsenges. Phys. Chem. **88**, 241 (1984); Chem. Phys. **90**, 257 (1984).
[28](a) J. L. Martins and W. Andreoni, Phys. Rev. B **28**, 3637 (1983); (b) W. Andreoni and J. L. Martins, Surf. Sci. **156**, 635 (1985).
[29]T. Ziegler, J. G. Snijders, and E. J. Baerends, J. Chem. Phys. **74**, 1271 (1981).
[30]For copper the parameter r_c defined in Ref. 14 is chosen to be $r_c=0.35$ a.u., to be compared with $r_c=0.20$ a.u. in Ref. 14. For Zn the two values are, respectively, $r_c=0.36$ a.u. and $r_c=0.19$ a.u.
[31]H. M. Hulburt and J. O. Hirschfelder, J. Chem. Phys. **9**, 61 (1941); **35**, 1901 (1961); see also A. C. Hurley, *Introduction to the Electron Theory of Small Molecules* (Academic, London, 1976), p. 8, for a discussion.
[32]M. Krauss and F. H. Mies, in *Excimer Lasers,* Vol. 30 of *Topics in Applied Physics,* edited by C. K. Rhodes (Springer-Verlag, New York, 1979).
[33]K. Rademann, B. Kaiser, U. Even, and H. Hensel, Phys. Rev. Lett. **59**, 2319 (1987); C. Brechignac *et al.*, *ibid.* **60**, 275 (1988).
[34]S. H. Linn, C. L. Liao, J. M. Brom, Jr., and C. Y. Ng, Chem. Phys. Lett. **105**, 645 (1984).
[35]R. J. Niefer *et al.*, Phys. Rev. B **35**, 4629 (1987).
[36]Preliminary computations for the IIB homonuclear dimers are discussed in R. O. Jones, J. Chem. Phys. **71**, 1300 (1979). Results for Zn_2 are also reported by J. Andzelm, E. Wimmer, and D. Salahub, in *The Challenge of d and f Electrons: Theory and Computation,* edited by D. R. Salahub and M. C. Zener, ACS Symposium Series (American Chemical Society, Washington, D.C., 1989).
[37]M. Posternak, G. Galli, and P. Ballone (unpublished).
[38]I. S. Gradshteyn and I. M. Ryzhik, *Table of Integrals, Series and Products* (Academic, New York, 1980), p. 737.
[39]Ching-Hua Su *et al.*, J. Chem. Phys. **81**, 11 (1984).
[40]R. D. van Zee, S. C. Blankespoor, and T. S. Zwier, J. Chem. Phys. **88**, 4650 (1988).